Hindawi
Mathematical Problems in Engineering
Volume 2020, Article ID 6096834, 11 pages
https://doi.org/10.1155/2020/6096834

Research Article

State Estimation of Lithium Batteries for Energy Storage Based on Dual Extended Kalman Filter

Xinming Xu,[1] Di Wu,[2] Lei Yang,[2] Huai Zhang,[3] and Guangjun Liu[2]

[1]*College of Mechanical and Electrical Engineering, Hunan Agricultural University, Changsha 410128, China*
[2]*School of Mechanical Engineering, Tongji University, Shanghai 200092, China*
[3]*Wuhu ChuRui Intelligent Technology Co., Ltd., Wuhu 241000, China*

Correspondence should be addressed to Guangjun Liu; gjliu@126.com

Received 28 January 2020; Accepted 5 March 2020; Published 11 April 2020

Academic Editor: Jerzy Baranowski

In general, battery packs are monitored by the battery management system (BMS) to ensure the efficiency and reliability of the energy storage system. SOC and SOH represent the battery's energy and lifetime, respectively. They are the core aspects of the battery BMS. The traditional method assumes that the SOC is determined by the integral of the current input and output from the battery over time, which is an open-loop-based approach and often accompanies by poor estimation accuracy and the accumulation of sensor errors. The contribution of this work is to establish a new equivalent circuit model based on the lithium battery external characteristic, and the battery parameters are identified by considering the influence of capacity fade, voltage rebound, and internal capacitance-resistance performance. The correlation between the ohmic internal resistance and real capacity is obtained by degradation test. Then, the dual extended Kalman filter (DEKF) is used to perform real-time prediction of the lithium battery state. And through the simulation analysis and experiments, the feasibility and precision of the estimation method are well proved.

1. Introduction

Lithium battery has been widely used in the energy storage field due to its high energy density, long cycle life, high voltage, and outstanding security [1]. In general, in order to ensure the efficiency and reliability of the energy storage system, battery packs are monitored by the battery management system (BMS). And the state estimation of the battery is the essential function of the BMS. The accurate online state estimation can contribute to monitor the battery's state of charge (SOC) and state of health (SOH) clearly so that the reasonable charge-discharge can be performed to keep its high-efficiency working conditions and long life [2].

SOC and SOH represent the battery's energy and lifetime, respectively. They are the core aspects of the battery BMS. The traditional method assumes that the SOC is determined by the integral of the current input and output from the battery over time. This is an open-loop-based approach, the result of which is often accompanied by poor estimation accuracy and the accumulation of sensor errors [3]. Moreover, in the past, the battery's capacity variations were not to be taken into account during the lifetime; thus, the estimation method had great deficiencies [4]. In fact, it comes with irreversible chemical reactions and physical changes in the working process of the battery, which make SOC and SOH tightly coupled with each other. Improper battery state estimation method can lead to premature damage and deterioration of the battery [5]. As the impedance and capacity of the battery change with time, the maximum power and energy that can be delivered by the battery will be reduced. This technical problem can be solved by simultaneously estimating the SOC and the SOH of the battery [6].

Traditional estimation methods, including the internal resistance method, coulomb counting (CC) method, open-circuit voltage method, and load charge method, have some limitations in practical application due to lack of abilities to correct errors and largely depending on high precision of sensors and low environment influences [7]. Nowadays, with

the development of modern control theory, there are some new algorithms which are constantly being used in battery state estimation. Plett [8] proposed the sigma-point Kalman filtering (SPKF) method as applied to BMS algorithms through the analysis of batteries' nonlinear characteristics. And a better result was obtained by comparison with the traditional Kalman filtering method. Fleischer et al. [9] presented a state-of-available-power prediction method based on the framework of the adaptive neuro-fuzzy inference system. The method achieved the accurate power prediction at low-temperature environment. Lee et al. [10] had researched the linear prediction error method and the neural network method in the battery state estimation and then found the latter had better precision in short-term prediction. Chen et al. [11] employed the genetic algorithm to estimate the battery model parameters based on analysis of the resistance-capacitance circuit model. The precision and robustness of results are much improved, but its real-time performance was limited.

The contribution of this paper is to establish a new equivalent circuit model based on the lithium battery external characteristic, and the battery parameters are identified by considering the influence of capacity fade, voltage rebound, and internal capacitance-resistance performance. The correlation between the ohmic internal resistance and real capacity is obtained by degradation test. Then, the dual extended Kalman filter (DEKF) is used to perform real-time prediction of the lithium battery state. And through the simulation analysis and experiments, the feasibility and precision of the estimation method are well proved.

The rest of the paper is organized as follows. An equivalent circuit model is established, and the characteristic parameters of the battery are identified in Section 2. In Section 3, the method of battery state estimation is proposed, and the computer-aided modeling analysis is carried out. Section 4 provides detailed experimental procedures and results. Section 5 presents some conclusions.

2. Battery Model and Parameter Identification

2.1. Battery Model. The battery performance is closely related to its internal parameters. And the change rule of characteristic parameters can be analyzed by establishing the reasonable equivalent model [12]. In order to achieve the real-time state analysis, not only the working characteristics, including voltage rebound effect, hysteresis, and electromotive force-SOC (EMF-SOC), need to be taken into consideration in the model but also the complex electrochemistry mechanism should be avoided as much as possible. Therefore, mainly focusing on the analysis of external characteristics, a new circuit containing a controlled source is established as the equivalent circuit model of the lithium battery. The model is based on Thevenin's theorem and consists of an equivalent voltage source and equivalent impedance, as shown in Figure 1.

2.1.1. The Equivalent Voltage Source. The voltage source is related with the SOC, SOH, and working conditions of the battery. Therefore, the equivalent voltage source E_B consists of electromotive force EMF and hysteresis voltage V_{h}. As the voltage-controlled voltage source (VCVS), EMF is controlled by voltage V_{SOC}. And C_{cap} is the capacity of the battery, which is related with the SOH. And the current flowing through C_{cap} is equal to the working current I_B. Therefore, the value of V_{SOC} can be used to represent the battery SOC:

$$V_{\mathrm{SOC}} = \frac{I_B t}{C_{\mathrm{cap}}} = \frac{C_{\mathrm{cap}} - C_{\mathrm{remain}}}{C_{\mathrm{cap}}}, \tag{1}$$

where t is the working time and C_{remain} is the remaining capacity.

Hysteresis voltage $V_{\mathrm{h}}$is also a voltage-controlled voltage source (VCVS), which is controlled by voltage V_{Lh}. The current flowing through inductance L_{h} is βI_{B}. Hysteresis voltage is influenced by previous working current, in which the characteristic can be described by a circuit containing the inductance. The value of V_{h} is determined by charging and discharging conditions:

$$V_{Lh} = L_{\mathrm{h}} \frac{\mathrm{d}(\beta I_{\mathrm{B}})}{\mathrm{d}t}. \tag{2}$$

Therefore, the equivalent voltage source is

$$E_B = \mathrm{EMF}(V_{\mathrm{SOC}}) + V_{\mathrm{h}}(V_{Lh}). \tag{3}$$

2.1.2. The Equivalent Impedance. The capacitance and resistance performance of the battery are described by an equivalent impedance submodel, which consists of the ohmic internal resistance R_Ω and *RC* capacitive-resistance network [13]. R_Ω is caused by materials and the specific structure of the battery, which will increase with the decay of SOH. And the *RC* capacitive-resistance network is used to describe the voltage rebound effect caused by polarization capacitance and polarization resistance [14]. The rebound performance of the model is closer to the real value of the lithium battery with higher the order of the network. Meanwhile, the complexity and computation time of the model will increase with the orders. Considering the accuracy of the model and the computational efficiency, the third-order *RC* is much reasonable. Then, according to zero-state response of the *RC* network, the polarization voltage $u_i(t)$ can be shown as

$$u_i(t) = R_i \cdot I_B(t) \cdot \left(1 - e^{-(t/R_i C_i)}\right), \quad i = 1, 2, 3. \tag{4}$$

Therefore, according to Thevenin's theorem, the complete equivalent circuit model of the lithium battery can be expressed as

$$u_B(t) = E_B(t) - \sum_{i=1}^{3} u_i(t) - I_B R_\Omega. \tag{5}$$

Through the equivalent circuit model, the relations of internal parameters and external working characteristic, including EMF-SOC, voltage hysteresis, rebound effect, and impedance characteristic of the lithium battery, can be described clearly.

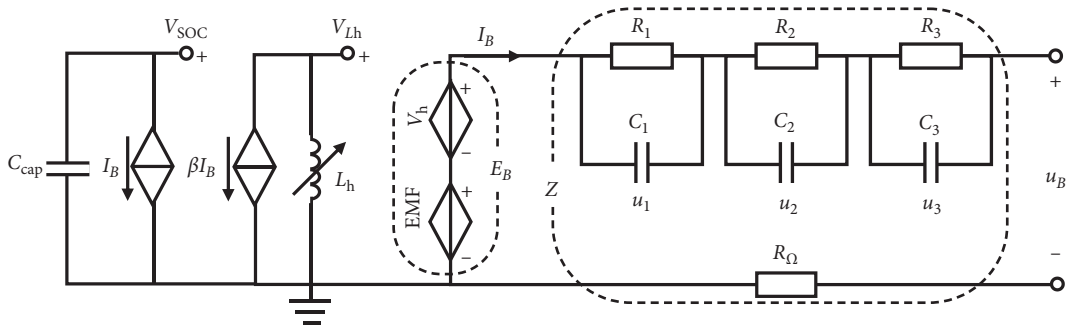

Figure 1: Equivalent circuit model of the lithium battery.

2.2. Parameter Identification. At the constant temperature of 25°C, a pulse discharge test for the max load 18650 lithium battery is performed to identify the model characteristic parameters. The battery capacity is 2900mAh, and the current is 2.9 A. The test current is shown in Figure 2(a). SOC and voltage u_B during the test are shown in Figure 2(b).

Based on the test data of the balance electromotive force E_B and corresponding SOC, the E_B – SOC characteristic curve can be obtained by the polynomial segmentation fitting method, as shown in Figure 3.

The corresponding mathematical expression is

$$f = \begin{cases} g_{11}x^4 + g_{12}x^3 + g_{13}x^2 + g_{14}x + g_{15} & (0.904, 1.000], \\ g_{21}x^4 + g_{22}x^3 + g_{23}x^2 + g_{24}x + g_{25} & (0.112, 0.904], \\ g_{31}x^4 + g_{32}x^3 + g_{33}x^2 + g_{34}x + g_{35} & [0.000, 0.112], \end{cases} \tag{6}$$

where G is the coefficient matrix, and

$$G = \begin{bmatrix} 8916.7 & -33285 & 46587 & -28975.1 & 6760.7 \\ 0.113 & -0.331 & 0.289 & 0.323 & 3.702 \\ -9204 & 2668 & -287.9 & 15.03 & 3.368 \end{bmatrix}. \tag{7}$$

The *RC*networks are in the zero-state respond during the voltage rebound period. Therefore, according to equation (5), the output voltage can be shown as

$$u_B(t) = E_B(t) - \Delta U_1 - \Delta U_2, \tag{8}$$

where ΔU_1 and ΔU_2 are, respectively, the rebound voltages in the first stage and second stage and can be expressed as

$$\Delta U_1 = I_B R_\Omega, \tag{9}$$

$$\Delta U_2 = b_1 e^{-\tau_1 t} + b_2 e^{-\tau_2 t} + b_3 e^{-\tau_3 t}, \tag{10}$$

where $b_i = R_i I_B$, $\tau_i = 1/C_i R_i$, $R_\Omega = \Delta U_1 / I_B$, and $(i = 1, 2, 3)$.

According to test data and equations (8)~(10), the voltage rebound characteristic curve can be obtained, as shown in Figure 4. And the parameters of the fitting curve are $b = [33.648 \ \ 23.136 \ \ 13.516]$ and $\tau = [4.4098 \ \ 0.0293 \ \ 0.0037]$. Therefore, the characteristic parameters of the battery can be identified, as shown in Table 1.

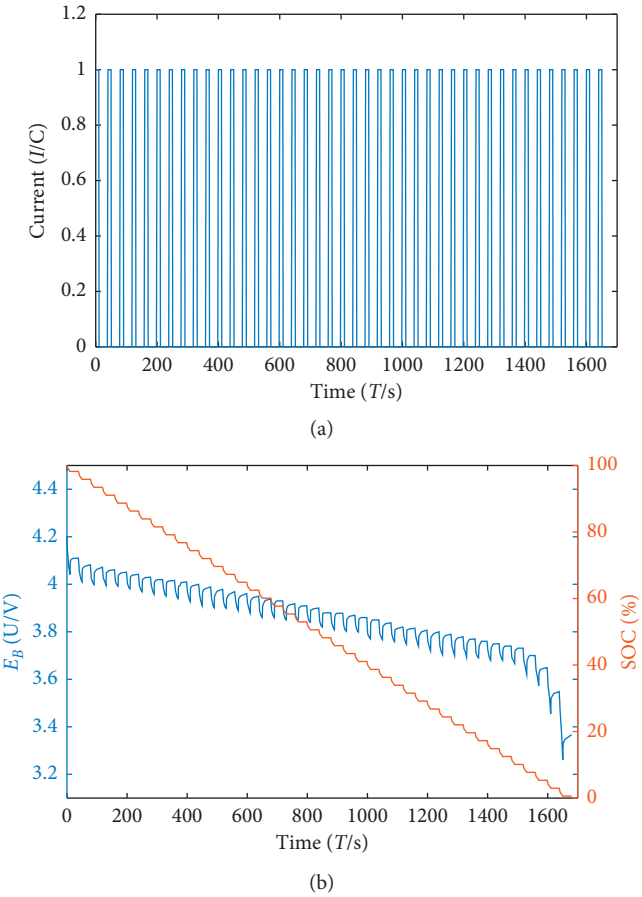

Figure 2: Pulse discharge test. (a) Test current. (b) Voltage and SOC.

3. Battery State Estimation

3.1. Battery State. Battery state contains the state of charge (SOC) and the state of health (SOH). SOC is the remain charge that can be released from the battery, which is related with the initial charge state, actual capacity, and previous current [15]:

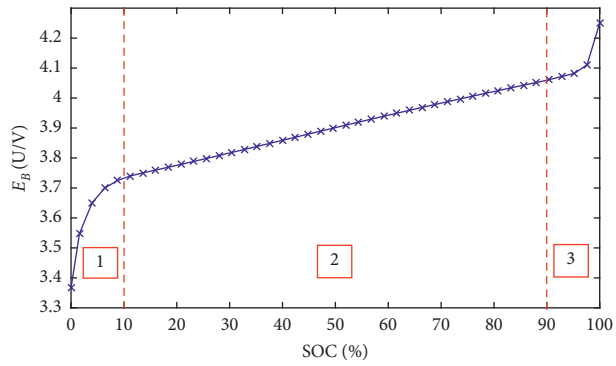

Figure 3: E_B – SOC characteristic curve.

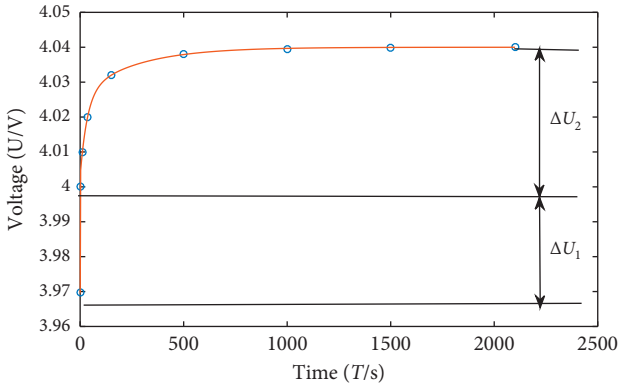

Figure 4: The rebound characteristic curve.

Table 1: The characteristic parameters.

R_Ω	R_1	R_2	R_3	C_1	C_2	C_3	C_{cap}
101 mΩ	65 mΩ	42 mΩ	24 mΩ	1258 F	268 F	1581 F	1.61 Ah

$$\text{SOC}(t) = \frac{Q_{\text{initial}} - \int_{t0}^{t} \eta I_B \mathrm{d}t}{C_{\text{cap}}^{\text{now}}} \times 100\%, \tag{11}$$

where Q^{initial} is the initial charge state and η is the coefficient of the current ratio.

SOH is evaluated based on the battery capacity. According to battery failure standard, the battery is invalid when its actual capacity drops to 80% of rated capacity [16]. Therefore, SOH can be defined as

$$\text{SOH} = \frac{C_{\text{cap}}^{\text{new}} - C_{\text{cap}}^{\text{now}}}{C_{\text{cap}}^{\text{new}} - C_{\text{cap}}^{\text{old}}} \times 100\%, \tag{12}$$

where $C_{\text{cap}}^{\text{new}}$,$C_{\text{cap}}^{\text{now}}$, and $C_{\text{cap}}^{\text{old}}$ are, respectively, the rated capacity, actual capacity, and invalid capacity.

The lithium ion in the electrolyte is hindered by the solid electrolyte interface (SEI) adhering to the electrode of the lithium battery. With continuous electrochemical reaction, SEI becomes thicker and thicker, which means hindrance to the lithium ion gets more serious. This can be seen from the increased ohmic internal resistance in the macroscopic view [17]. Therefore, the battery capacity gradually decreases, and ohmic internal resistance increases during the battery degradation [18]. In the normal working condition, battery degradation is a long-term and slow process. In this work, the changes of the ohmic internal resistance and capacity are obtained by accelerating the growth of solid electrolyte membranes in the high-temperature working environment. The $C_{\text{cap}}^{\text{now}} - R_\Omega$ degradation curve is shown in Figure 5.

The corresponding mathematical expression is

$$C_{\text{cap}}^{\text{now}} = 17163R_\Omega^3 - 1924R_\Omega^2 + 49R_\Omega - 1. \tag{13}$$

According to the result analysis, SOC and SOH are closely related. The estimation accuracy of SOC can be improved by considering the influence of capacity degradation.

3.2. Estimation Principle of DEKF. Extended Kalman filter (EKF) is an improved method based on the traditional Kalman filter that can be used for the estimation of nonlinear state variables [19]. And when two sets of state variables need to be estimated, dual extended Kalman filtering (DEKF) can be used [20]. In this work, the battery SOC is estimated, which is related with the polarization resistances. The state variable is defined as $X = \begin{bmatrix} \text{SOC} & u_1 & u_2 & u_3 \end{bmatrix}^T$. Besides, SOH can be used to calculate the actual capacity to improve the estimation accuracy of SOC. Although SOH cannot be measured directly, it can be obtained by the estimation of the ohmic internal resistance R^{Ω} due to equation (13). So, another state variable is defined as $Y = [R_\Omega]^{\text{T}}$. Besides, an observable variable related with state variables is needed in Kalman filter [21]. According to the battery model, the output voltage can be regarded as the observational variable $Z = u^{\text{B}}$ for it can be measured by a sensor directly. The measuring equation at time k is shown as

$$u_B^k = f\left(X_1^k\right) - X_2^k - X_3^k - X_4^k - R_\Omega^k I_B^k + v^k, \tag{14}$$

where $f(X_1^k)$ is the E_B – SOC characteristic equation and v^k is the measurement noise.

The battery state estimation based on the DEKF method is shown in Figure 6.

According to the result of the last cycle, the battery capacity at time k can be updated. Then, based on the equivalent circuit model, state equations are established, and the preliminary state predictions X^{k*} and Y^{k*} are calculated by

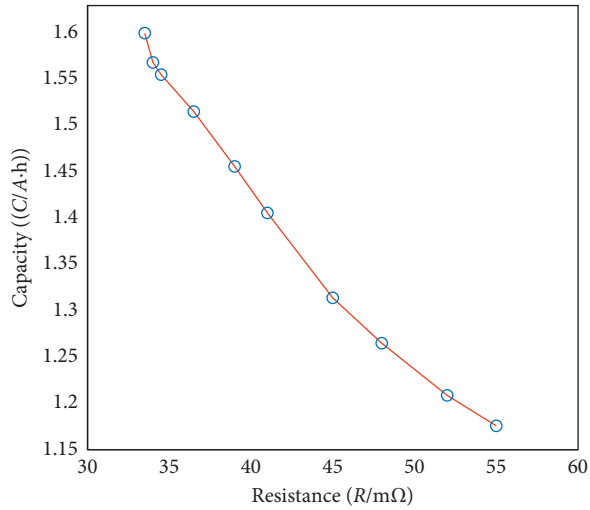

Figure 5: $C_{cap}^{now} - R_{\Omega}$ degradation curve.

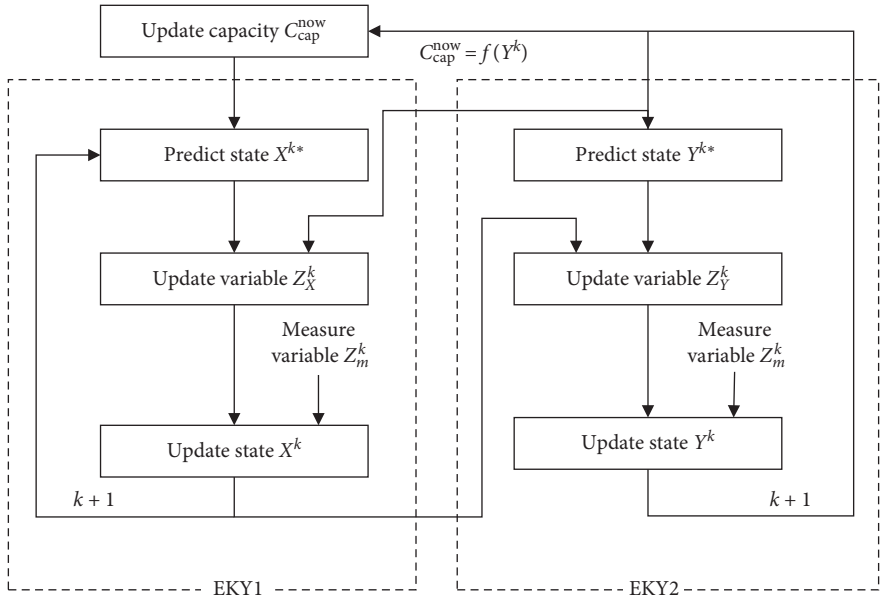

Figure 6: DEKF procedure for state estimation.

$$X^{k*} = \begin{bmatrix} 1 & 0 & 0 & 0 \\ 0 & \frac{R_s C_s}{R_s C_s + 1} & 0 & 0 \\ 0 & 0 & \frac{R_m C_m}{R_m C_m + 1} & 0 \\ 0 & 0 & 0 & \frac{R_l C_l}{R_l C_l + 1} \end{bmatrix} X^{k-1} + \begin{bmatrix} \frac{1}{C_{cap}} \\ \frac{R_s}{R_s C_s + 1} \\ \frac{R_m}{R_m C_m + 1} \\ \frac{R_l}{R_l C_l + 1} \end{bmatrix} I_B^{k-1} + \omega^{k-1},$$

$$Y^{k*} = Y^{k-1} + r^{k-1}, \tag{15}$$

where I_B^{k-1} is the process variable, ω^{k-1} is the process noise, and r^{k-1} is the small perturbation of state Y^k. And $[X^{k*}, Y^{k*}]$ is the preliminary estimation of state variables.

The estimated values obtained by state equations cannot avoid the accumulation of process errors. Besides, the initial errors that may exist is hard to be recognized and corrected [22]. Therefore, an observable variable Z needs to be established to correct the previous error. This is the key to the algorithm. In the DEKF method, both of the two state variables need to be corrected by the observational variable:

$$\begin{cases} X^k = X^{k*} + K_X^k \left(Z_M^k - Z_X^k\right), \\ Y^k = Y^{k*} + K_Y^k \left(Z_M^k - Z_Y^k\right). \end{cases} \tag{16}$$

The error corrections depend on the difference value of observational variable $(Z_M^k - Z^k)$ and the Kalman gain K^k. $Z_M^k = u^k$ is obtained by the voltage sensor, and Z^k is calculated by the measuring equation. The Kalman gain K^k is calculated by

$$\begin{cases} K_X^k = P_X^{k*} H_X^{kT} \left(H_X^k P_X^{k*} H_X^{kT} + R_X^k\right)^{-1}, \\ K_Y^k = P_Y^{k*} H_Y^{kT} \left(H_Y^k P_Y^{k*} H_Y^{kT} + R_Y^k\right)^{-1}, \end{cases} \tag{17}$$

where R^k are the covariances of measurement noise that rely on the performance of the sensor. H^k Jacobian matrixes of state variables are shown in equation (18). P^{k*} are the covariance matrixes of the state, which are used to reflect the change of state variables, as shown in equation (19).

$$\begin{cases} H_X^k = \dfrac{\partial u_B^k}{\partial X} = \left[\dfrac{\partial f\left(X_1\right)}{\partial X_1} \;\; -1 \;\; -1 \;\; -1 \right], \\ H_Y^k = \dfrac{\partial u_B^k}{\partial Y} = -I_B^k, \end{cases} \tag{18}$$

$$\begin{cases} P_X^{k*} = AP^{k-1}A^T + Q_X^{k-1}, \\ P_Y^{k*} = P^{k-1} + Q_Y^{k-1}, \end{cases} \tag{19}$$

where Q^{k-1} are the covariances of the process noise.

3.3. Simulation Model and Analysis. The real cycle test is time consuming. And it is more efficient for the algorithm analysis to simulate the battery working conditions with the help of computer simulation technique [23]. Therefore, according to the principle of the battery equivalent circuit, a simulation model is established by using mathematical logic modules and circuit element modules in Matlab Simulink, as shown in Figure 7. In order to ensure the reliability of simulation analysis and reflect the real working characteristics of the battery, the parameters of the simulation model are set up corresponding with Table 1.

The SOC estimation is performed by using the DEKF method in the 1C intermittent discharge working condition as shown in Figure 8. The measurement noise and process noise are simulated by Gaussian white noises. According to the sensor performance, the noise covariances are set as $Q = 0.039$ and $R = 2.5 \times 10^{-5}$. To consider the ability of error correction, four situations are simulated, where the initial errors are, respectively, set as 0%, 5%, 10%, and 15%, and the step size k is 0.5s. The simulation results are shown in Figure 9.

In Figure 9, the initial errors of DEKF1~ DEKF4 are, respectively, 0%, 5%, 10%, and 15%. It is seen that, with the discharge process, in the DEKF1 situation, which has no initial error, the estimation is still near the real value. And in terms of DEKF2~ DEKF4 that contain different initial errors, their estimations are gradually close to real value. Therefore, the results show that DEKF has good convergence and stability and can correct the initial errors in the state estimation of the battery.

4. Experiment

4.1. Experimental Setup. To verify the feasibility and accuracy of the DEKF method in the real SOC estimation, the experiments are performed by the BMS circuit. The circuit structure consists of a lithium battery pack, the battery monitoring circuit (BMC), the battery control unit (BCU), and the upper computer, as shown in Figure 10(a). In the experiment, the battery pack consists of 12 MAX LOAD 18650 cells connected in series. The LTC6804-1 chip is used to monitor the battery data. BCU is a Linduino microcontroller. The upper computer and BCU are communicated by the serial peripheral interface (SPI), as shown in Figure 10(b). The load is a resistor, and the current is controlled by a sliding rheostat.

The SOC estimation experiments are performed by, respectively, using the traditional CC method and DEKF method in the working conditions of the open-circuit state, constant-current discharge state, and intermittent discharge state.

4.2. Results and Discussion

4.2.1. Open-Circuit State. When the initial charge is 92%, the SOC estimation is performed in the open-circuit state. The measuring voltage nearly remains constant due to the zero working current, as shown in Figure 11. When initial error is 0, the SOC estimated by both methods is close to 92% with a little fluctuate, as shown in Figure 12(a). Because the current is zero, CC-SOC and REAL-SOC have the same value at this time, and the two curves are basically coincident. And when 2% initial error exists, the SOC estimated by the DEKF method can converge to real value, but the estimation still contains initial error by using the CC method as shown in Figure 12(b).

4.2.2. Constant-Current Discharge State. The measuring voltage constantly decreases in 1.5 C constant-current discharge state, as shown in Figure 13. It is seen that the gradient is great in the high and low SOC stages, while the gradient is much less in the middle stages, which reflects the E_B – SOC characteristic of the lithium battery. When initial error is 0, the SOC estimated by the DEKF method is near

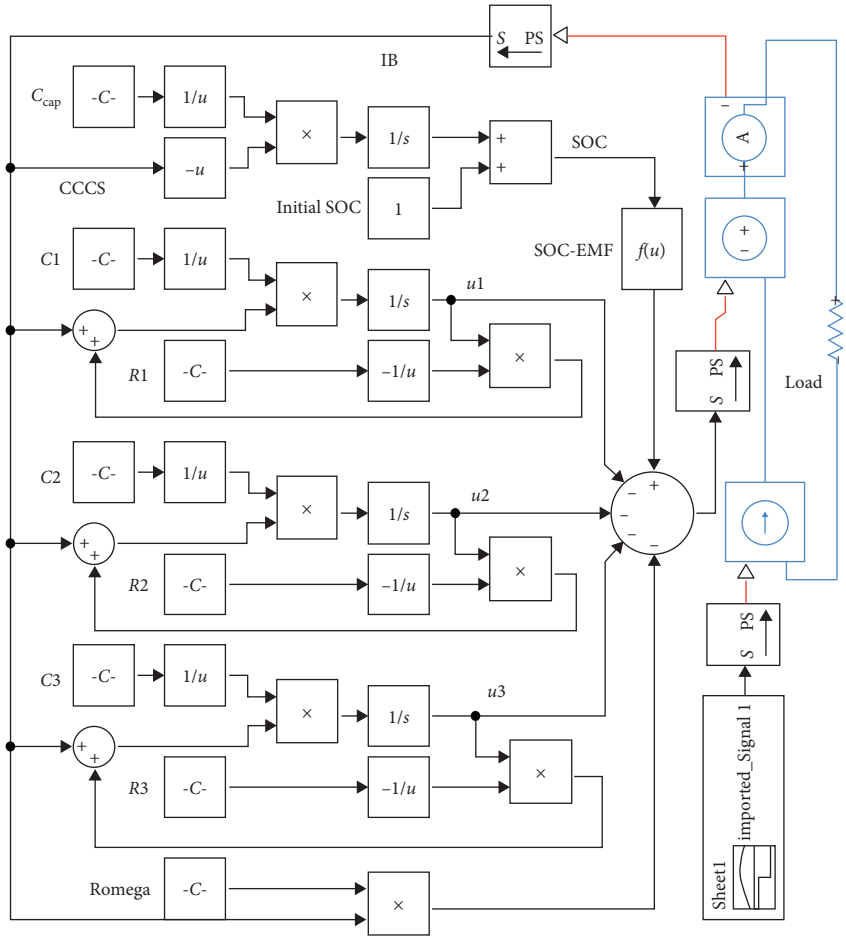

Figure 7: The battery simulation model.

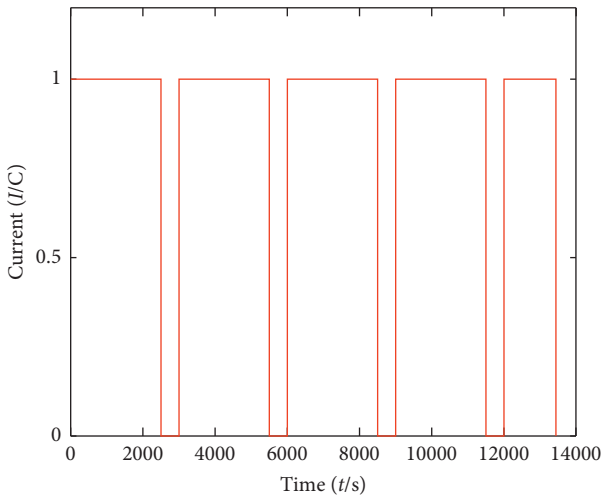

Figure 8: The simulated discharge condition.

the real value, while the value by the CC method gradually deviated from the real value, as shown in Figure 14(a). And when 10% initial error is introduced, the estimation of the CC method still contains nearly whole error, while the error is reduced obviously by the DEKF method, as shown in Figure 14(b).

4.2.3. Intermittent Discharge State. The change of measuring voltage in 1C intermittent discharge state is shown in Figure 15. It is seen that the voltage is in a decreasing tendency, but some rebounds and step changes occur in the intermittent phase due to the rebound characteristic of the battery.

When initial errors are 0 and 10%, the estimation results of SOC are shown in Figure 16. It is seen that the SOC can keep track with real value both in cutoff and discharge stage, while the CC method is serious influenced by errors.

4.2.4. Error Analysis. In the open-circuit state, the accuracy of the CC method completely depends on initial error because of zero working current, while DEKF can correct error within a short time. In working conditions, even if the initial error is 0, the maximum errors of CC, respectively, reach 8% and 12%, while the DEKF method is less than 2%. In terms of situation that 10% initial error is introduced, and the error of the CC method is still very big in all of the experiment processes. But, the DEKF method has good convergence, and the initial error can gradually be decreased by correction of the state equation and observational equation.

The average errors of two methods in different conditions are shown in Table 2. It is seen that whatever the

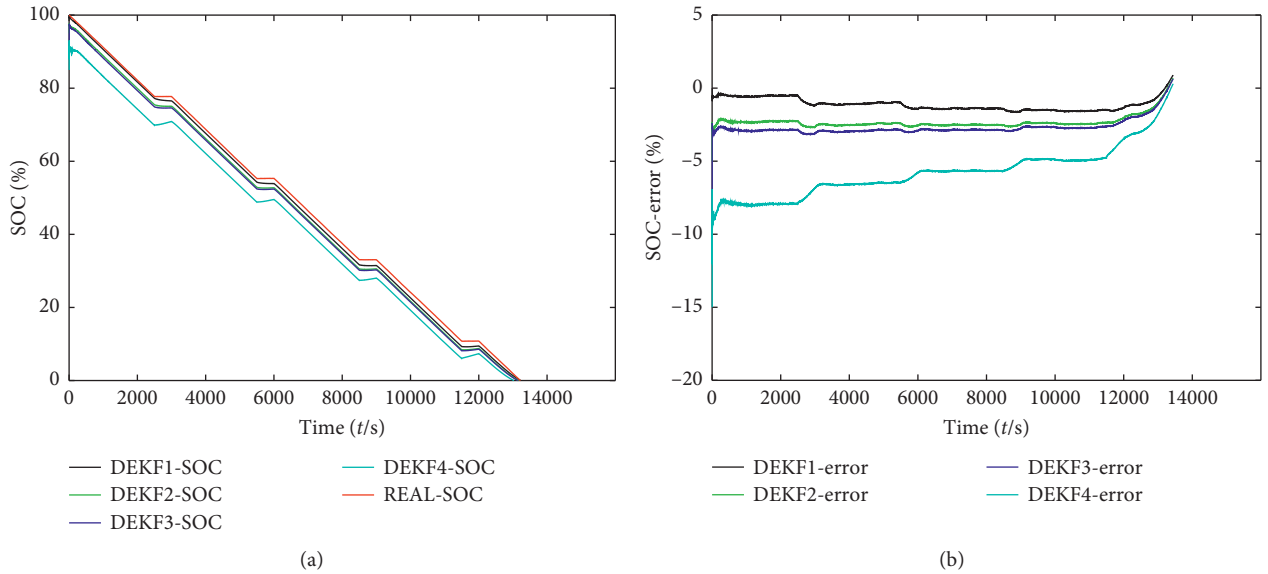

Figure 9: The simulation results. (a) SOC. (b) Estimation errors.

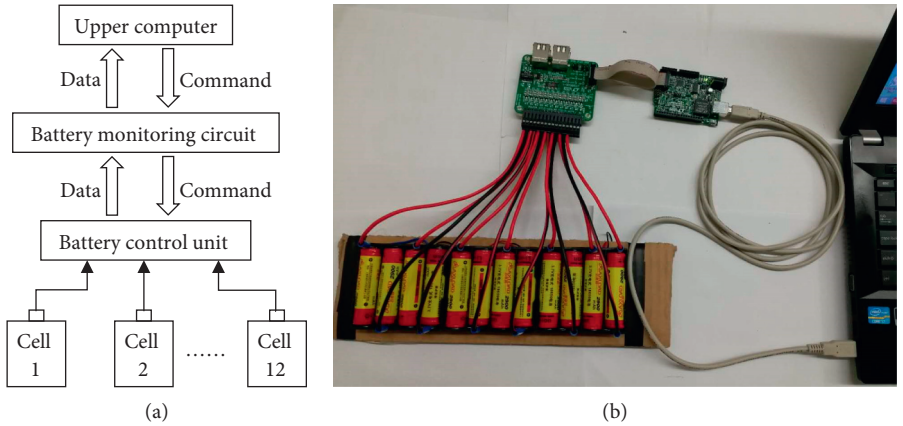

Figure 10: Experimental circuit and its structure. (a) The circuit structure. (b) Experimental setup.

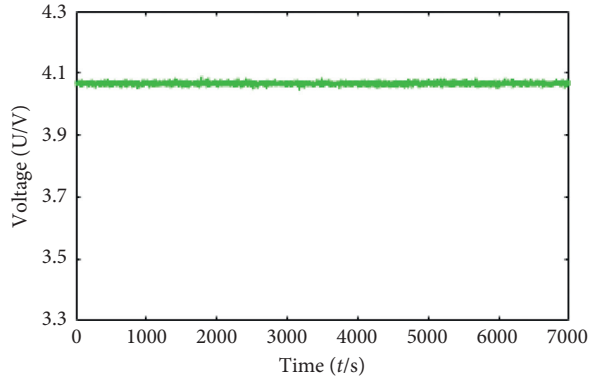

Figure 11: Measuring voltage in the open-circuit state.

initial errors exist or not, average errors of DEKF are less than 2.7%, which is also much less than the errors of the CC method. Besides, the DEKF has good robustness and can well deal with the influence of initial errors, while the CC method much relies on the stable initial value and the precision of sensors. Therefore, it is proved that the DEKF performs well in the SOC estimation of the lithium battery.

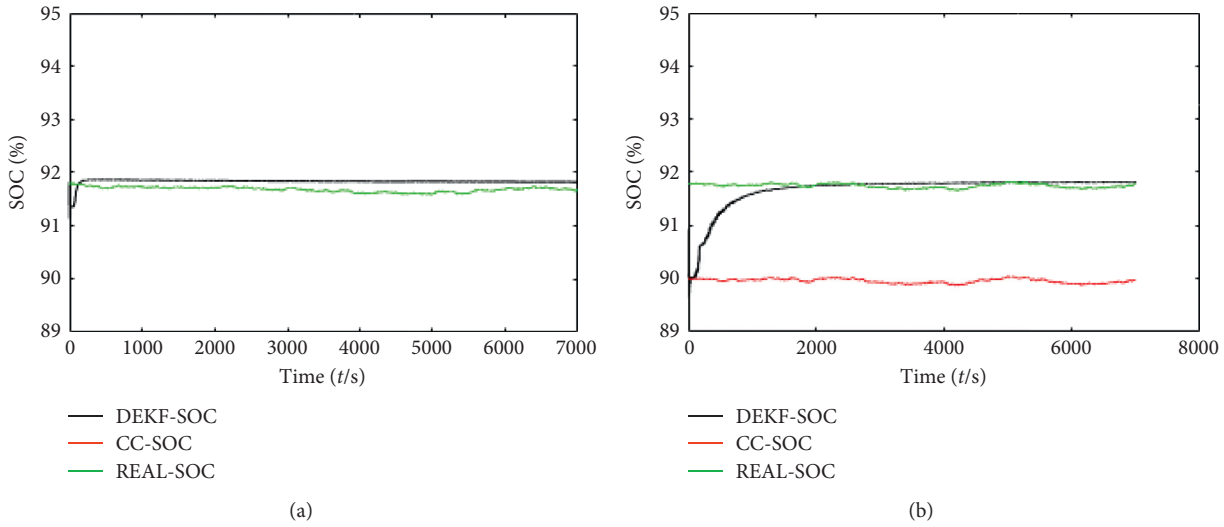

Figure 12: SOC estimation in the open-circuit state. (a) 0 initial error. (b) 2% initial error.

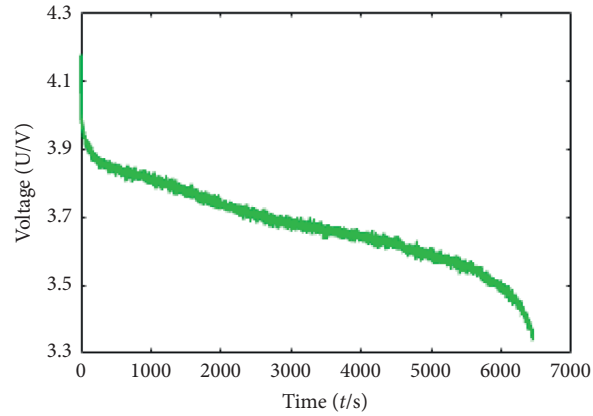

Figure 13: Measuring voltage in the constant-current discharge state.

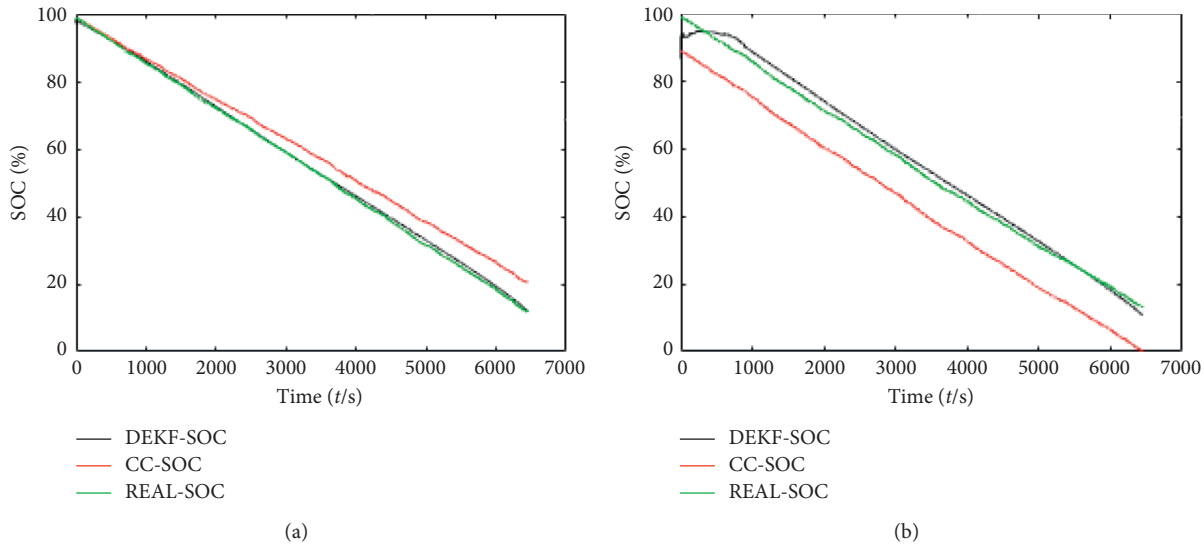

Figure 14: SOC estimation in the constant-current discharge state. (a) 0 initial error. (b) 10% initial error.

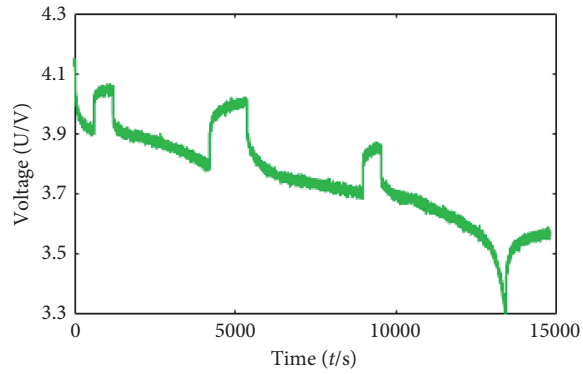

Figure 15: Measuring voltage in the intermittent discharge state.

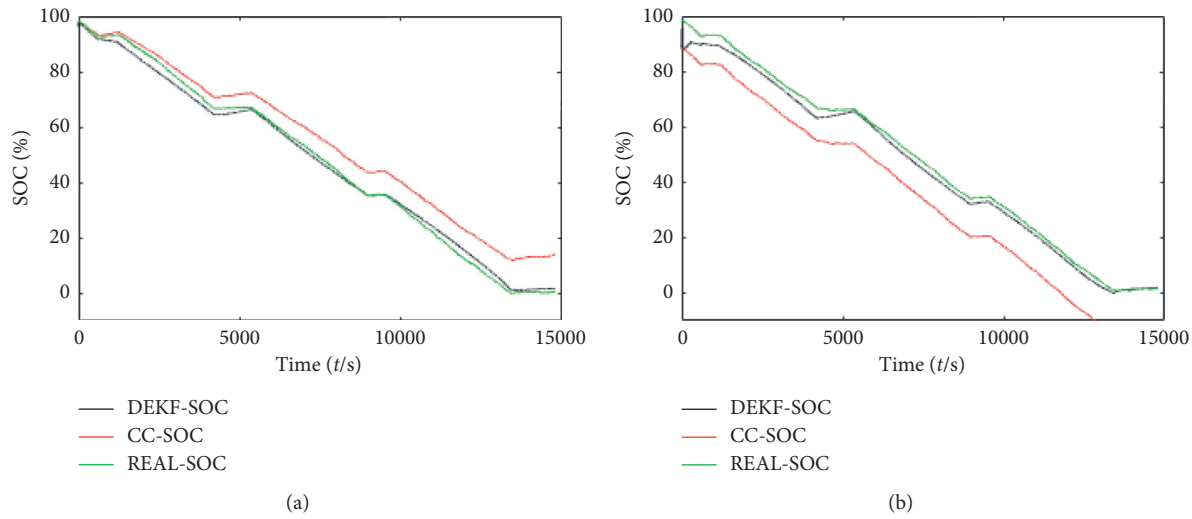

Figure 16: SOC estimation in the intermittent discharge state. (a) 0 initial error. (b) 10% initial error.

Table 2: The average estimation error.

	Open-circuit state		Constant-current discharge state		Intermittent discharge state	
	0 initial error (%)	2% initial error (%)	0 initial error (%)	10% initial error (%)	0 initial error (%)	10% initial error (%)
DEKF	0.2	0.2	0.8	1.3	1.8	2.7
CC	0	1.8	4.2	11.4	6.5	13.3

5. Conclusions

(1) A new equivalent circuit model that can describe the working characteristics of the lithium battery is established based on Thevenin's theorem. The internal parameters, including capacity, the ohmic internal resistance, polarization resistance, and capacitance, are identified by fitting characteristic curve. The relation of equivalent internal resistance and capacity is obtained by battery life experiments.

(2) The DEKF principle using in battery state estimation is analyzed based on the relation of SOC and SOH. A simulation model is established to analyze the estimation ability with the influence of different initial errors.

(3) The SOC estimation experiments are performed by, respectively, using the traditional CC method and DEKF method in three different working conditions. By comparison with the estimation results of the CC method, the results of DEKF are still near the real values, even if the errors of sensors exist. When 10% initial errors are introduced, the DEKF can correct the errors, and the estimation can fast converge to real values. The average errors are less than 3% in all kinds of working conditions, which verifies the feasibility of the algorithm.

Data Availability

The data used to support the findings of this study are available from the corresponding author upon request.

Conflicts of Interest

The authors declare that there are no conflicts of interest regarding the publication of this paper.

Acknowledgments

The authors would like to acknowledge the support of the National Key R&D Program of China (Grant no. 2016YFC0802900) and the Fundamental Research Funds for the Central Universities.

References

[1] L. Croguennec and M. R. Palacin, "Recent achievements on inorganic electrode materials for lithium-ion batteries," *Journal of the American Chemical Society*, vol. 137, no. 1, pp. 3140–3156, 2015.

[2] S. Zhang, L. Yang, X. Zhao, and J. Qiang, "A GA optimization for lithium-ion battery equalization based on SOC estimation by NN and FLC," *International Journal of Electrical Power & Energy Systems*, vol. 73, pp. 318–328, 2015.

[3] R. Xiong, Q. Yu, L. Y. Wang, and C. Lin, "A novel method to obtain the open circuit voltage for the state of charge of lithium ion batteries in electric vehicles by using H infinity filter," *Applied Energy*, vol. 207, pp. 346–353, 2017.

[4] Y. Li, K. Liu, A. M. Foley et al., "Data-driven health estimation and lifetime prediction of lithium-ion batteries: a review," *Renewable and Sustainable Energy Reviews*, vol. 113, pp. 68–85, 2019.

[5] Y. Xing, W. He, M. Pecht, and K. L. Tsui, "State of charge estimation of lithium-ion batteries using the open-circuit voltage at various ambient temperatures," *Applied Energy*, vol. 113, pp. 106–115, 2014.

[6] B. Sun, J. Jiang, F. Zheng et al., "Practical state of health estimation of power batteries based on Delphi method and grey relational grade analysis," *Journal of Power Sources*, vol. 282, pp. 146–157, 2015.

[7] Z. Yuan, X. Hu, H. Ma, and S. E. Li, "Combined State of Charge and State of Health estimation over lithium-ion battery cell cycle lifespan for electric vehicles," *Journal of Power Sources*, vol. 273, pp. 793–803, 2015.

[8] G. L. Plett, "Extended Kalman filtering for battery management systems of LiPB-based HEV battery packs: Part 1. Introduction and state estimation," *Journal of Power Sources*, vol. 161, no. 2, pp. 1356–1368, 2004.

[9] C. Fleischer, W. Waag, Z. Bai, and D. U. Sauer, "Adaptive online state-of-available-power prediction of lithium-ion batteries," *Journal of Power Electronics*, vol. 13, no. 4, pp. 516–527, 2013.

[10] S. Lee, H. Cui, M. Rezvanizaniani, and J. Ni, "Battery prognostics: SoC and SoH prediction," in *Proceedings of the ASME 2012 International Manufacturing Science and Engineering Conference Collocated with the, North American Manufacturing Research Conference and in Participation with the International Conference on Tribology Materials and Processing*, pp. 689–695, Notre Dame, IN, USA, July 2013.

[11] Z. Chen, C. C. Mi, Y. Fu, J. Xu, and X. Gong, "Online battery state of health estimation based on Genetic Algorithm for electric and hybrid vehicle applications," *Journal of Power Sources*, vol. 240, no. 31, pp. 184–192, 2013.

[12] M. Shen and Q. Gao, "A review on battery management system from the modeling efforts to its multiapplication and integration," *International Journal of Energy Research*, vol. 43, no. 10, pp. 5042–5075, 2019.

[13] C. Chen, R. Xiong, R. Yang, W. Shen, and F. Sun, "State-of-charge estimation of lithium-ion battery using an improved neural network model and extended Kalman filter," *Journal of Cleaner Production*, vol. 234, no. 10, pp. 1153–1164, 2019.

[14] J. Jiang, H. Ruan, B. Sun et al., "A reduced low-temperature electro-thermal coupled model for lithium-ion batteries," *Applied Energy*, vol. 177, pp. 804–816, 2016.

[15] C. Zhang, L. Y. Wang, X. Li, W. Chen, G. G. Yin, and J. Jiang, "Robust and adaptive estimation of state of charge for lithium-ion batteries," *IEEE Transactions on Industrial Electronics*, vol. 62, no. 8, pp. 4948–4957, 2015.

[16] A. E. Mejdoubi, A. . Oukaour, H. Chaoui, H. Gualous, J. Sabor, and Y. Slamani, ""State-of-charge and state-of-health lithium-ion batteries' diagnosis according to surface temperature variation," *IEEE Transactions on Industrial Electronics*, vol. 63, no. 4, pp. 2391–2402, 2015.

[17] J. Cannarella and C. B. Arnold, "State of health and charge measurements in lithium-ion batteries using mechanical stress," *Journal of Power Sources*, vol. 269, no. 2, pp. 7–14, 2014.

[18] A. Guha and A. Patra, "State of health estimation of lithium-ion batteries using capacity fade and internal resistance growth models," *IEEE Transactions on Transportation Electrification*, vol. 4, no. 1, pp. 135–146, 2018.

[19] G. Pérez, M. Garmendia, J. F. Reynaud, J. Crego, and U. Viscarret, "Enhanced closed loop State of Charge estimator for lithium-ion batteries based on Extended Kalman Filter," *Applied Energy*, vol. 155, pp. 834–845, 2015.

[20] S. Koga, L. Camacho-Solorio, and M. Krstic, "State estimation for lithium ion batteries with phase transition materials," in *Proceedings of the ASME 2017 Dynamic Systems and Control Conference*, Tysons Corner, VA, USA, October 2017.

[21] Y. Chen, Y. Ma, and H. Chen, "State of charge and state of health estimation for lithium-ion battery through dual sliding mode observer based on AMESim-Simulink co-simulation," *Journal of Renewable and Sustainable Energy*, vol. 10, no. 3, Article ID 034103, 2018.

[22] L. Lu, X. Han, J. Li, J. Hua, and M. Ouyang, "A review on the key issues for lithium-ion battery management in electric vehicles," *Journal of Power Sources*, vol. 226, pp. 272–288, 2013.

[23] P. Shrivastava, T. K. Soon, M. Y. I. B. Idris, and S. Mekhilef, "Overview of batteries State of Charge estimation methods," *Renewable and Sustainable Energy Reviews*, vol. 113, Article ID 109233, 2019.